Materials Today Bio 32 (2025) 101687

Contents lists available at ScienceDirect

Materials Today Bio

journal homepage: www.journals.elsevier.com/materials-today-bio

Injectable hydrogel microsphere orchestrates immune regulation and bone regeneration via sustained release of calcitriol

Jiajun Chen [a,b,c], Xingrui Yan [a,b,c], Li Nie [a,b,c], Siqi Zhou [a,b,c,d,e], Ping Ji [a,b,c], Hongmei Zhang [a,b,c,*]

[a] Stomatological Hospital of Chongqing Medical University, Chongqing, 401147, China
[b] Chongqing Key Laboratory of Oral Diseases and Biomedical Sciences, Chongqing, 401147, China
[c] Chongqing Municipal Key Laboratory of Oral Biomedical Engineering of Higher Education, Chongqing, 401147, China
[d] Chongqing University Affiliated Renji Hospital, Chongqing, 400062, China
[e] The Fifth People's Hospital of Chongqing, Chongqing, 400062, China

ARTICLE INFO

Keywords:
Hydrogel microspheres
Polydopamine
Calcitriol
Immunomodulation
Bone regeneration

ABSTRACT

Repairing bone defects in inflammatory conditions remains a significant clinical challenge. An ideal scaffold material for such situations should enable minimally invasive implantation and integrate capabilities for immunomodulation, anti-infection therapy, and enhanced bone regeneration. In this study, we developed injectable calcitriol@polydopamine@gelatin methacryloyl hydrogel microspheres (CAL@PDA@GMs) using microfluidic technology. This system facilitates the sustained release of calcitriol, which features excellent biocompatibility and biodegradability, promotes osteogenesis, scavenges excessive reactive oxygen species (ROS), and induces the polarization of macrophages from the M1 to M2 phenotype, thereby mitigating lipopolysaccharide (LPS)-induced inflammation. These mechanisms work synergistically to create an optimal immune microenvironment for bone regeneration in inflammatory conditions. RNA sequencing (RNA-Seq) analyses revealed that immunomodulation is achieved by regulating macrophage phenotypes, inhibiting the nuclear transcription factor-kappa B (NF-κB) and ROS signaling pathways, and reducing the secretion of pro-inflammatory cytokines. This study proposes a novel method to enhance tissue regeneration by remediating the damaged tissue microenvironment and presents a potential clinical therapeutic strategy for large-scale bone injuries.

1. Introduction

The reconstruction of large-scale bone defects caused by severe periodontitis, trauma, or tumor excision represents a substantial clinical obstacle [1–3]. The current gold standard involves bone grafting with autografts and allografts, which presents several drawbacks, such as infection risk, transplant rejection, donor scarcity, and donor site morbidity [4,5]. Advances in bone tissue engineering have paved the way for the development of artificial bone repair materials with adjustable properties, providing novel alternatives for bone defect treatment [6]. Nevertheless, certain materials may provoke acute foreign body reactions or prolonged inflammatory responses, leading to healing failures [7]. Consequently, osteo-immunomodulation, a strategy that harmonizes the interplay between immune and bone cells, has emerged as a promising new frontier for bone defect restoration [2].

Macrophages play a crucial role in host immune responses, polarizing into either M1 (pro-inflammatory) or M2 (anti-inflammatory) phenotypes based on the specific conditions of the local microenvironment [8]. Regulating macrophage polarization toward the M2 phenotype is beneficial to alleviating local inflammation, creating a favorable immune microenvironment for bone regeneration [8]. Despite extensive research into materials that modulate macrophage polarization for immunomodulatory impacts in transplant regions, issues such as drug inactivation, complications, high expenses, and intricate production processes remain [9]. Developing a novel, economically feasible material that maintains steady drug delivery, promotes bone regeneration, mitigates inflammation, and regulates macrophage polarization from M1 to M2 could significantly enhance bone reconstruction by optimizing immunomodulation and improving tissue regeneration.

Calcitriol [1,25-dihydroxy vitamin D3, 1,25(OH)2D3], the most

* Corresponding author. Stomatological Hospital of Chongqing Medical University, Chongqing, 401147, China.
E-mail address: hmzhang@hospital.cqmu.edu.cn (H. Zhang).

https://doi.org/10.1016/j.mtbio.2025.101687
Received 12 March 2025; Accepted 19 March 2025
Available online 20 March 2025

active final metabolite of vitamin D3, plays a pivotal role in regulating calcium homeostasis, bone metabolism, and immune responses [10]. Research indicates that calcitriol enhances bone regeneration and possesses anti-inflammatory properties. It promotes osteoblast differentiation and maturation, upregulating osteogenic differentiation markers [11–13]. Additionally, it demonstrates both anti-inflammatory and antioxidative effects, which counteract the suppression of osteogenesis by inflammation: calcitriol downregulates cytokines triggered by LPS, such as interleukin *(IL)-6* and *IL-8,* and activates the endogenous antioxidant system, protecting osteoblasts from oxidative stress [14–16]. Consequently, extensive research has been conducted to investigate the application of osteoarthritis, osteoporosis, and other conditions. Local administration of calcitriol has efficiently promoted osteogenesis *in vivo* [17,18], indicating its potential as a bioactive agent for topical use in addressing bone defects.

Dopamine (DA), renowned for its excellent biocompatibility, stands out as the most prevalent catecholamine neurotransmitter within the brain. Polydopamine (PDA), a polymer derived from DA, boasts robust adhesive properties, which facilitate drug loading via physical adsorption, primarily through π-π stacking interactions [19]. This characteristic also allows for sustained drug release in targeted environments [20]. Past research has utilized PDA for loading various bioactive components, including trypsin, bovine serum albumin (BSA), and antibodies [21,22], suggesting its potential for calcitriol encapsulation. Gelatin methacryloyl (GelMA), a derivative of gelatin that resembles the extracellular matrix, offers superior cell-signaling capabilities and biodegradability, creating a conducive environment for a diverse range of cell types. [23,24]. It can be crafted into hydrogel scaffolds with diverse morphologies and characteristics under different processing conditions and has been the subject of extensive research for bone defect repair [25]. Hydrogel microspheres fabricated using microfluidic technology are characterized by their uniform size, minimal volume, and ability to be administered via needle injection in a minimally invasive fashion, making them suitable for complex, irregular, and minor bone defects. These microspheres possess a large surface area, facilitating the exchange of oxygen and nutrients between cells and the extracellular microenvironment and promoting cell viability [26–29]. Moreover, the integration of bioactive ingredients further enhances the wound healing process.

Based on the above advantages, we fabricated GelMA hydrogel microspheres (GMs) using microfluidic technology as scaffolds for PDA nanoparticles (PDA NPs) loaded with calcitriol, creating a biomaterial CAL@PDA@GMs that releases calcitriol sustainably (Scheme 1A). We evaluated their biocompatibility, osteogenic potential, and anti-inflammatory effects by assessing their impact on attachment, proliferation, osteogenic differentiation, and mineralization in terms of bone marrow mesenchymal stem cells (BMSCs) *in vitro* (Scheme 1B). Furthermore, we assessed their modulatory effects on macrophage polarization by observing the behavior of RAW 264.7 cells under inflammatory conditions *in vitro* (Scheme 1B). Finally, we investigated their immunomodulatory function and osteogenic effect on bone regeneration *in vivo*, utilizing cranial and femoral defect models (Scheme 1C). This study presents an innovative strategy for integrating immunomodulation, anti-inflammation, and bone regeneration but also offers a potential clinical treatment approach for large-scale bone injuries.

2. Results and discussion

2.1. Characterization of CAL@PDA@GMs

Based on the outstanding biocompatibility, robust adhesion, high drug loading capacity, and reliable biodegradability [19,22], we synthesized PDA to encapsulate calcitriol, forming CAL@PDA. This compound was subsequently integrated with GMs to fabricate

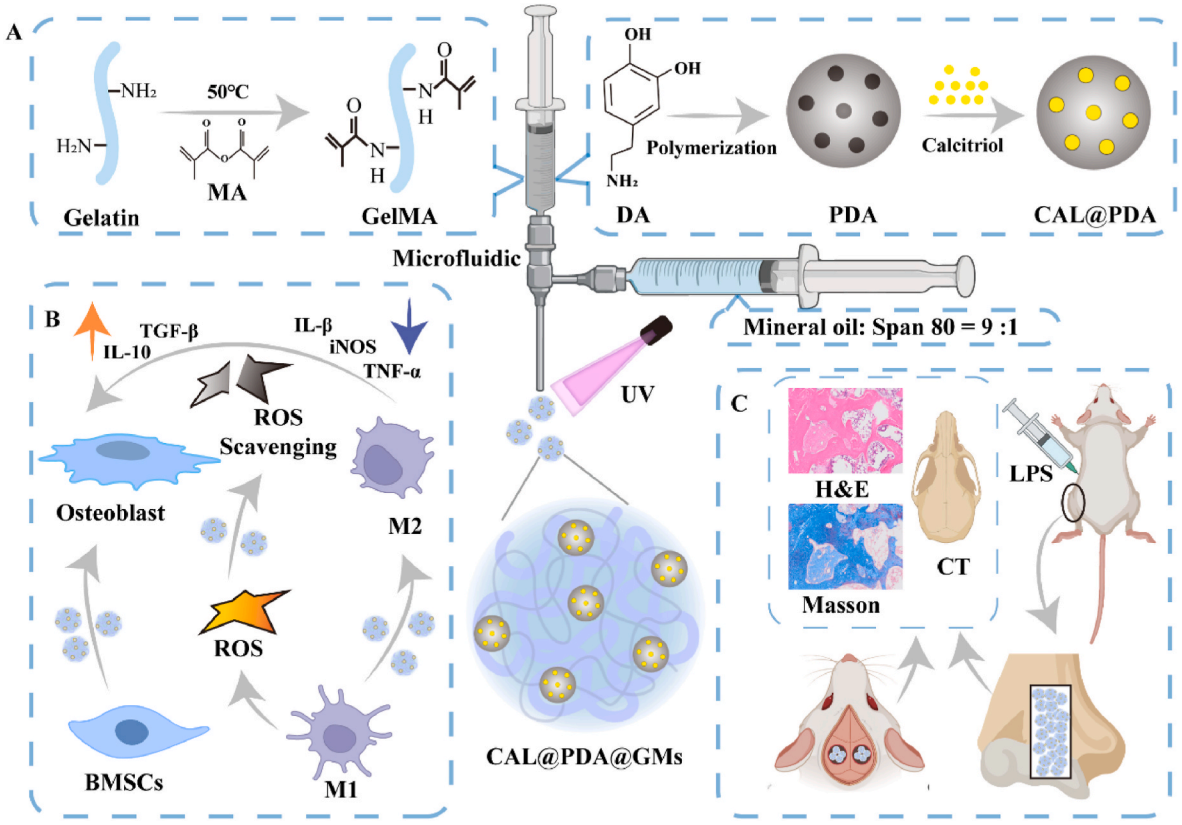

Scheme 1. Schematic illustration of A) the synthesis of CAL@PDA and GelMA for the fabrication of CAL@PDA@GMs using microfluidic technology, B) the osteogenesis and immunomodulation effects of CAL@PDA@GMs, and C) its application in repairing cranial and femoral defects in rats.

CAL@PDA@GMs using microfluidic technology. Scanning electron microscopy (SEM) showed that PDA and CAL@PDA exhibited a spherical morphology (Fig. 1A). The PDA particles had a rough surface texture, with a mean diameter of 376.76 ± 33.20 nm (Fig. 1D). In contrast, CAL@PDA displayed a smoother surface, and its average diameter was determined to be larger at 412.76 ± 75.80 nm (Fig. 1B and E). Moreover, the CAL@PDA@GMs were characterized by a porous, honeycomb-like microstructure on their surface, within which the CAL@PDA nanoparticles were embedded (Fig. 1C). We measured the porosity of the microsphere by SEM images and analyzed it with Image J, the data showed that the porosity of the microsphere was 74.30 % ± 0.81 % [30,31]. This honeycomb-like porous microstructure was essential for maintaining cell viability during tissue regeneration. It offered sufficient space for cell adhesion, growth, and expansion while facilitating the interchange of oxygen and nutrients between the cells and their immediate microenvironment [26–29,32]. The average diameter of the CAL@PDA@GMs was 149.45 ± 10.62 μm (Fig. 1F), which permitted the microsphere to pass through a 23G needle [32], maintaining its shape without any deformation or damage (Fig. S1). In addition, energy-dispersive spectroscopy (EDS) was utilized to examine the elemental makeup of CAL@PDA@GMs [32,33]. The results showed that the material contained C (36.3 %), N (22.4 %), and O (41.3 %) (Fig. S2). The proton-1 nuclear magnetic resonance (^{1}H NMR) spectrum of supernatant from the degradation of CAL@PDA@GMs, as shown in Fig. 1G, the characteristic peaks corresponding to calcitriol confirmed the successful fabrication of the CAL@PDA@GMs.

Studies that have employed calcitriol either locally or systemically have largely failed to achieve sustained release of the compound [17,18,34]. Since the ultraviolet (UV) absorption peak of GelMA is similar to calcitriol (Fig. S3), we detected the release curve of CAL@PDA in phosphate-buffered saline (PBS). Fig. 1H showed the release of calcitriol was rapid in the initial 10 h, reaching approximately 13.55 % ± 0.02 %, then tended towards stability, with a cumulative release of 37.12 % ± 0.06 % over 30 days (Fig. 1I). This indicated that CAL@PDA's capability of continuously releasing calcitriol provided the advantage of local application. We detected that calcitriol has a maximum absorption peak at 299 nm wavelength (Fig. S4). According to this, we get the standard curve of absorbance versus concentration of calcitriol under UV light (Fig. 1J), shown with an R^2 value of 0.9983, confirming the reliability of the formula. We verified the effect of calcitriol concentration on the expression of ALP in BMSCs, which showed that the concentration of calcitriol from 10^{-5} M to 10^{-12} M can promote the expression of ALP in

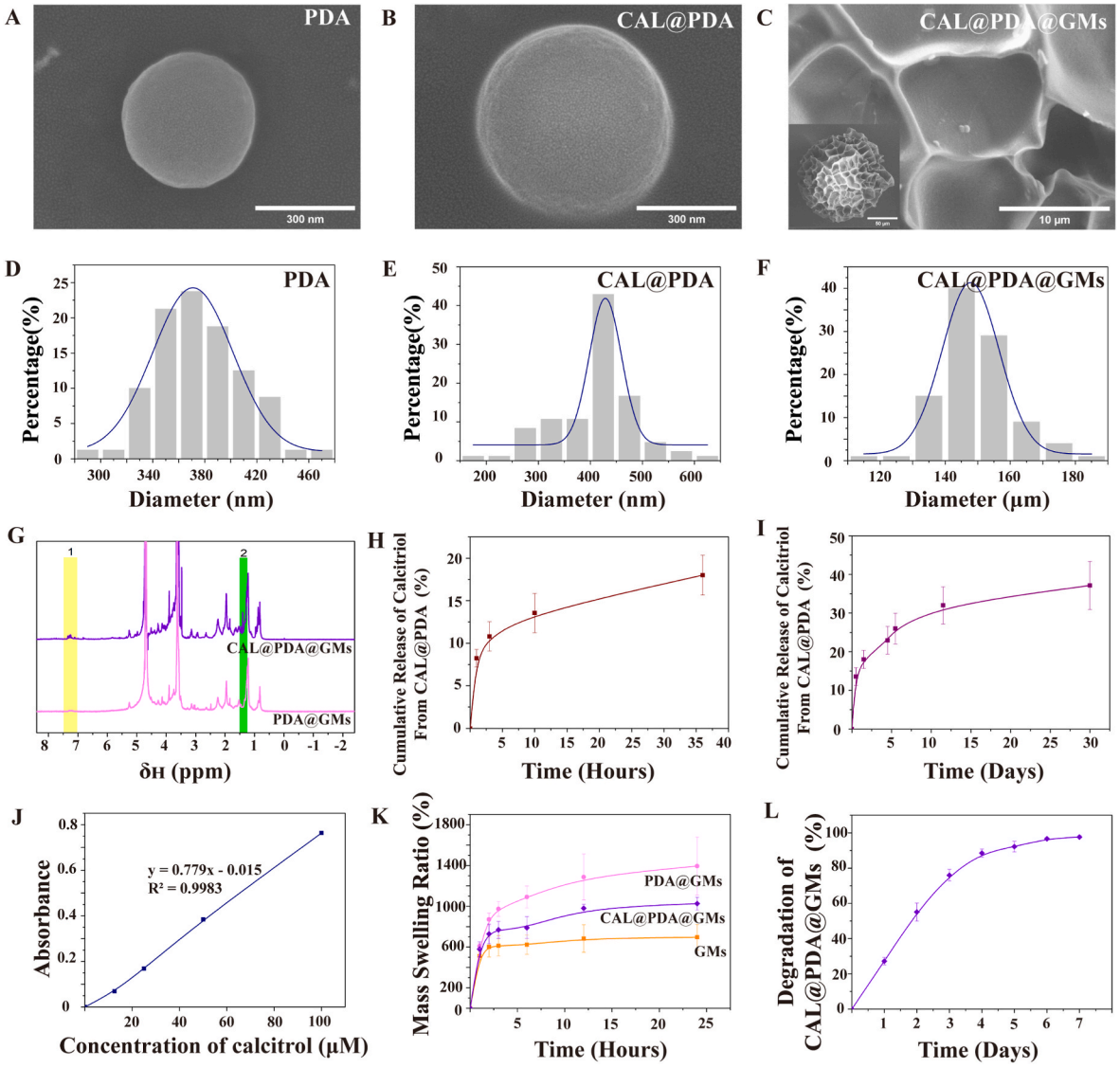

Fig. 1. Characterization of PDA, CAL@PDA, and CAL@PDA@GMs. A) SEM images of PDA, B) CAL@PDA, and C) CAL@PDA@GMs. D-F) Diameter distribution. G) ^{1}H NMR spectra of CAL@PDA@GMs degraded supernatant. H-I) Drug release profiles of CAL@PDA. J) Standard curve of absorbance and concentration of calcitriol. K) Mass swelling ratio. L) Degradation rate of CAL@PDA@GMs. Scale bar: 300 nm (A, B), 50 and 10 μm (C).

BMSCs (Figs. S5 and S6). Based on the drug release curve, the concentration of calcitriol released from the CAL@PDA@GMs was within this range, suggesting that the CAL@PDA@GMs could sustain a biological effect over time. A reasonable swelling ratio could provide a humid environment and enhance the transport of nutrients and the diffusion of oxygen, which is essential for cell viability [35]. Fig. 1K illustrates evident swelling attributable to water absorption in the GMs, PDA@GMs, and CAL@PDA@GMs within the first hour, followed by a gradual plateau. The appropriate degradation of the hydrogel microspheres was critical for cell migration and infiltration to facilitate tissue regeneration and drug release[36]. We added 0.1 U/mL collagenase II to PBS to investigate the degradation profile of GMs, as depicted in Fig. 1L. The CAL@PDA@GMs degraded within 7 days *in vitro*. Live/dead cell staining (Fig. 2A) and the CCK-8 assay (Fig. 2C) revealed a progressive increase in cell density over the 7-day culture period. Furthermore, cytoskeleton staining utilizing phalloidin demonstrated a gradual increase in cell attachment to the microspheres over time (Fig. 2B and D). In conclusion, an injectable hydrogel microsphere with favorable biocompatibility, appropriate biodegradability, and capacity to sustain release calcitriol was fabricated successfully, which is beneficial for

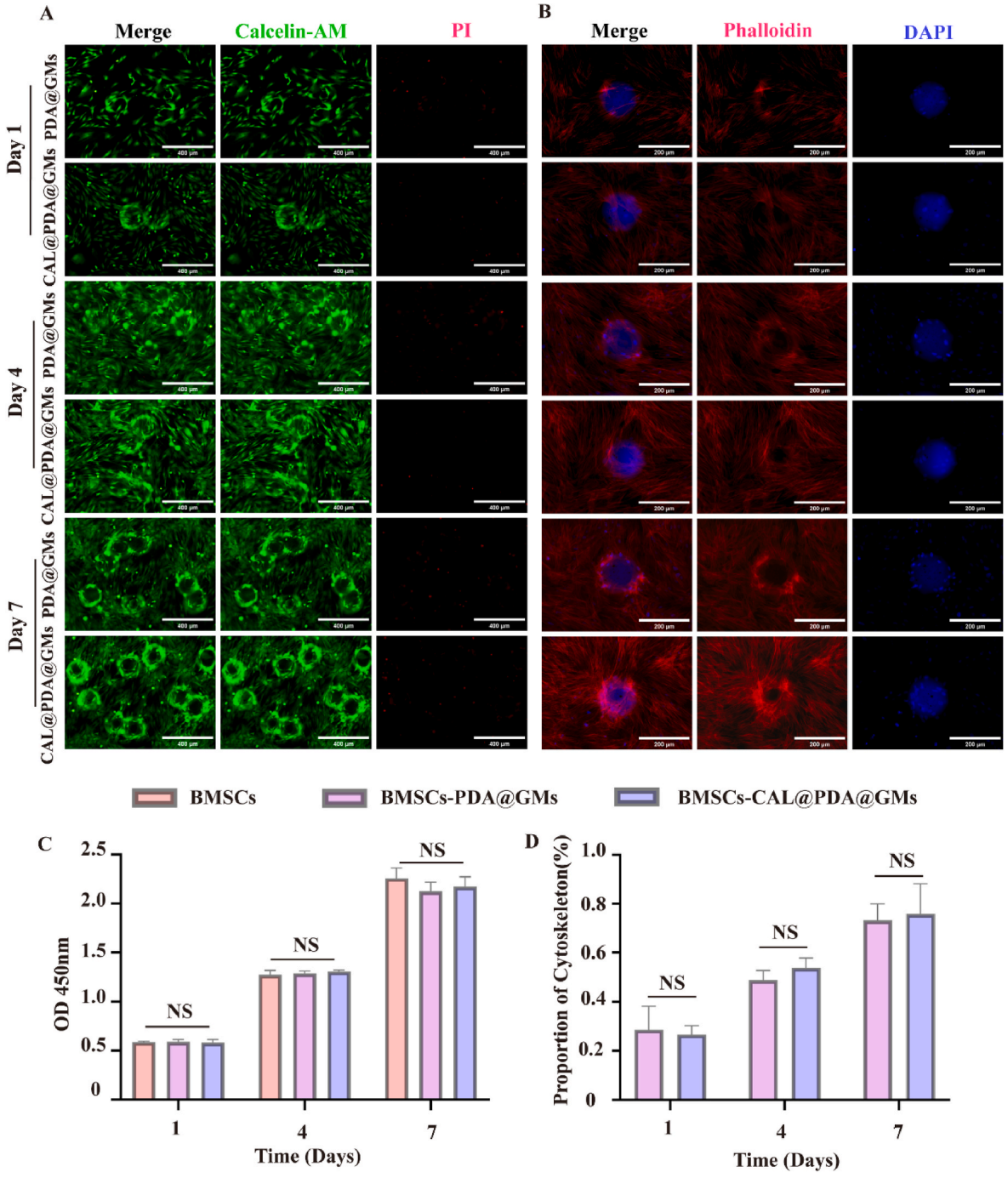

Fig. 2. Biocompatibility of CAL@PDA@GMs. A) Representative fluorescence images of live/dead staining in PDA@GMs and CAL@PDA@GMs. B) Cytoskeleton staining with phalloidin of PDA@GMs and CAL@PDA@GMs. C) The optical density (OD) value in the control PDA@GMs and CAL@PDA@GMs detected via CCK8 assay. D) Percentage of adhesion area of cells on GMs. Scale bar: 400 μm (A), 200 μm(B). Data are presented as the mean ± SD, NS indicates no significant differences.

advancing subsequent research endeavors.

2.2. Osteogenic evaluation in vitro and in vivo

2.2.1. Osteogenic differentiation of BMSCs in vitro

In addition to their favorable cytocompatibility, the osteogenic potential of bioactive materials significantly contributes to expediting the repair of bone defects since osteoblast differentiation is essential for directing bone regeneration [37]. To evaluate the osteogenic differentiation and mineralization, we conducted assessments of alkaline phosphatase (ALP) activity, alizarin red staining (ARS), and the expression of osteogenic-related genes [osteopontin (*Opn*), *Alp*, collagenase I (*Col-I*), runt-related transcription factor 2 (*Runx2*), osteocalcin (*Ocn*)] using quantitative real-time polymerase chain reaction

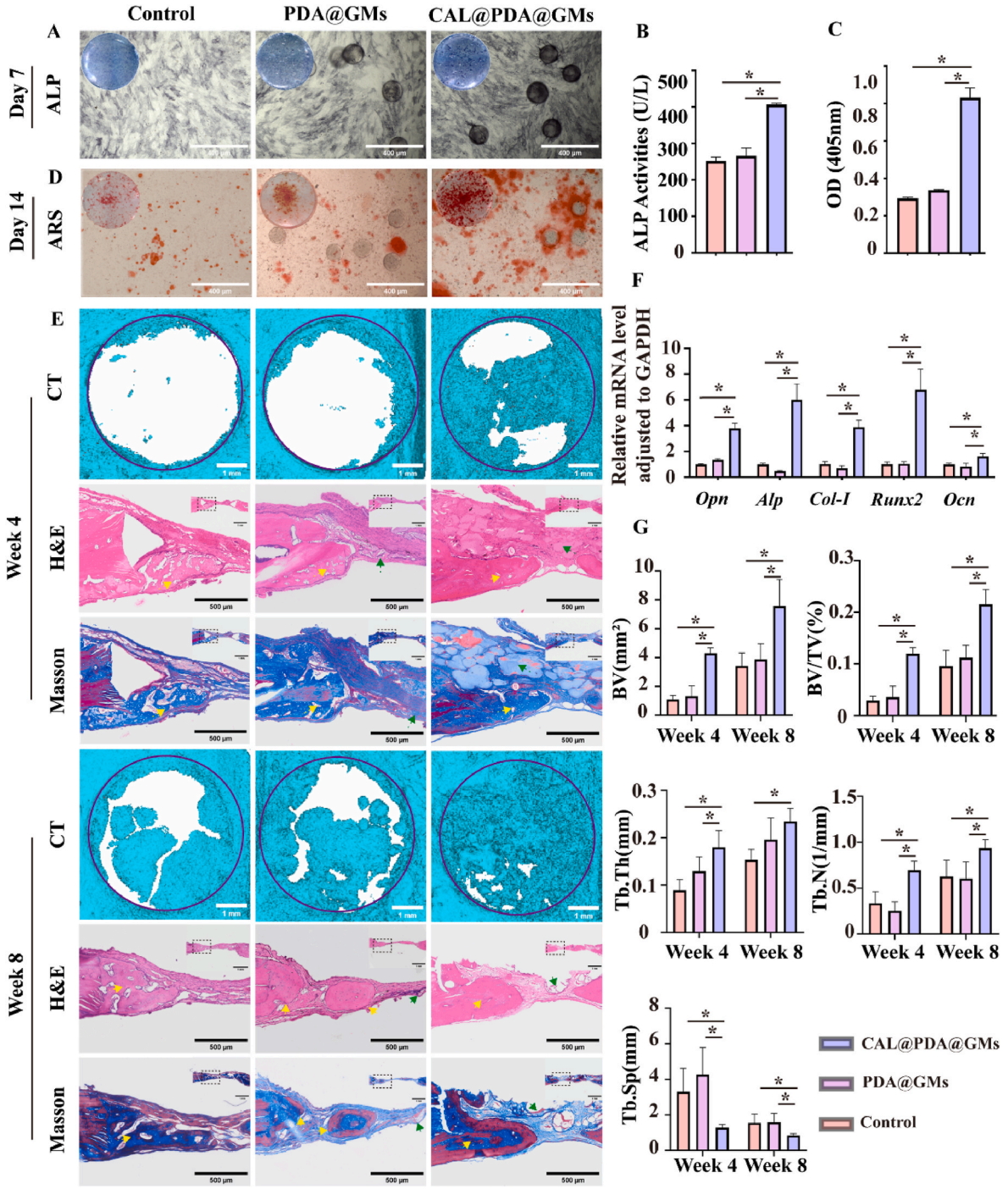

Fig. 3. Osteogenic differentiation of BMSCs *in vitro* and bone regeneration in the rat skull defect model *in vivo*. A) Microscopic images and B) quantitative analysis of ALP staining on day 7. C) Quantitative analysis and D) microscopic images of ARS staining on day 14. E) Representative micro-CT images, H&E, and Masson staining of new bone formation in the defect area 4 and 8 weeks after implantation. F) Gene expression of osteogenesis-related markers (*Opn*, *Alp*, *Col-I*, *Runx2*, and *Ocn*). G). Quantitative analysis of micro-CT parameters (BV, BV/TV, Tb. N, Tb. Th and Tb. Sp) of regenerated bone in the defect area. The blue circles represent the defect region with a diameter of 5 mm. Yellow arrow: newly formed bone tissue. Green arrow: hydrogel. Scale bar: 400 μm (A, D). 1 mm and 500 μm (E). Data are presented as the mean ± SD. $*p < 0.05$ indicates significant differences. (For interpretation of the references to colour in this figure legend, the reader is referred to the Web version of this article.)

(qRT-PCR). The ALP (Fig. 3A and B) and ARS (Fig. 3C and D) analyses showed that the CAL@PDA@GMs significantly enhanced ALP expression as well as the deposition of calcium salt and nodules. The qRT-PCR results showed a considerable upregulation of osteogenesis-related genes (*Opn*, *Alp*, *Col-I*, *Runx2*, and *Ocn*) after 7 days of co-culture with CAL@PDA@GMs (Fig. 3F). These results imply that CAL@PDA@GMs effectively facilitate the early-stage osteogenic differentiation and mineralization of BMSCs *in vitro*.

2.2.2. Bone reconstruction and regeneration in vivo

To assess the osteogenic potential of CAL@PDA@GMs *in vivo*, we induced two circular transosseous defects (diameter $\varphi = 5$ mm) on the rat skull to establish a rat skull bone defect model (Fig. S7). Micro-CT 3D-reconstructed images and quantitative analysis of new bone formation revealed a significant enhancement in bone regeneration in the CAL@PDA@GMs group at 4 and 8 weeks. Notably, the CAL@PDA@GMs facilitated bone tissue growth from the periphery toward the center of the defect sites (Fig. 3E). Detailed morphometric analysis of the micro-CT data, including bone volume (BV), bone volume/tissue volume (BV/TV), the number of trabeculae (Tb. N), trabeculae thickness (Tb. Th), and the trabecular separation (Tb. Sp), further substantiated these observations (Fig. 3G). H&E and Masson's trichrome staining (Fig. 3E) also demonstrated increased new bone formation (indicated by yellow arrows) in the CAL@PDA@GMs group. In addition, the gradual degradation of the hydrogel microspheres (indicated by the green arrow), replaced by newly formed bone, suggested their good compatibility and long-term biodegradability *in vivo* (Fig. 3E). This biodegradability is conducive to sustained bone ingrowth and provides ongoing mechanical support within the bone defect areas. Moreover, *in vivo* toxicity assessments of the CAL@PDA@GMs against the heart, liver, spleen, lungs, and kidneys revealed no significant tissue toxicity (Fig. S8). These findings underscore the outstanding osteogenic capabilities of CAL@PDA@GMs *in vitro and in vivo*.

2.3. Osteogenic evaluation in an inflammatory environment in vitro and in vivo

2.3.1. Osteogenic differentiation of BMSCs in an inflammatory environment in vitro

Injuries and diseases produce an inflammatory state that hinders the pro-regenerative environment, leading to bone resorption and suppression of bone tissue repair, which ultimately adversely affects the osseointegration of implants *in vivo* [37,38]. Although CAL@PDA@GMs exhibit excellent osteogenic properties, their performance in inflammatory microenvironments has not been previously investigated. Therefore, we designed experiments to evaluate the osteogenic effects of CAL@PDA@GMs under inflammatory conditions. Studies have shown that LPS-induced inflammation resulted in excessively high levels of inflammatory cytokines around the prosthesis, which increased osteoclast formation and impaired osteogenic activity [39]. To simulate an inflammatory environment *in vitro*, we added LPS to the culture medium. ALP (Fig. 4A and B) and ARS (Fig. 4C and D) analyses showed that the LPS inhibited ALP expression, calcium salt deposition and nodule formation, whereas the CAL@PDA@GMs significantly mitigated these inhibitory effects. qRT-PCR revealed that LPS down-regulated osteogenesis-related genes (*Opn*, *Alp*, *Col-I*, *Runx2*, and *Ocn*) on day 7, a suppression that was counteracted by CAL@PDA@GMs (Fig. 4E). In the LPS group, the inflammation-related gene *IL-6* and tumor necrosis factor-α (*TNF-α*) were up-regulated, while anti-inflammatory genes transforming growth factor-β (*TGF-β*) were down-regulated. In contrast, the CAL@PDA@GMs group exhibited the opposite trend (Fig. 4F). These results indicate that CAL@PDA@GMs relieve inflammation and promote osteogenic differentiation and mineralization of BMSCs in an inflammatory environment *in vitro*.

2.3.2. Bone reconstruction and regeneration in inflammation in vivo

To induce an inflammatory condition *in vivo*, rats were injected with LPS for 7 days, resulting in a significant increase in the total white blood cell (WBC) count and neutrophil count (NEUT) in the rats, while the red blood cell (RBC), hemoglobin (HGB), and platelet counts (PLT) remained stable (Table S2). Subsequently, we created a cylindrical bone defect with a diameter of 2 mm and a depth of 5 mm in the distal metaphysis of the femur to establish a femoral defect model, aiming to investigate the effects of CAL@PDA@GMs on bone defect healing within an inflammatory environment (Fig. S9). The micro-CT 3D-reconstructed images and quantitative analysis (Fig. 4G and H) revealed the CAL@PDA@GMs groups exhibited a marked increase in new bone formation, as evidenced by the BV, BV/TV, and Tb. N, Tb. Th and Tb. Sp at 4 and 8 weeks postoperatively. H&E and Masson's trichrome staining (Fig. 4G) demonstrated a substantial amount of new bone tissue growth and infiltration within the hydrogel matrix in the CAL@PDA@GMs groups, indicating the material's ability to facilitate cell ingrowth and promote material-tissue integration under inflammatory conditions. Given that macrophages are instrumental in the inflammatory response and subsequently influence the outcome of bone healing [40], their activation was assessed through *in vivo* immunofluorescence staining. As depicted in Fig. S10, the control group exhibited a substantial presence of macrophages expressing pro-inflammatory M1 markers (red, CCR7+) alongside a minor population displaying anti-inflammatory M2 markers (green, CD206). Conversely, the CAL@PDA@GMs group presented a reversed scenario 4 weeks into the postoperative period. This aligns with research demonstrating that some bioactive scaffolds can polarize the macrophage into the M2 phenotype, thereby mitigating the inflammation and fostering bone regeneration within 4 weeks [41–46]. The bone repair process typically spans 6–10 weeks, during which M2 phenotype macrophages continue to play a role [43,47–49]. In our study, the bone defect was repaired at 8 weeks, at which point we still observed a small number of macrophages (Fig. S10).

The findings above indicate that CAL@PDA@GMs are efficacious in reducing inflammation and facilitating the repair of bone defects within an inflammatory context. This therapeutic effect may be partially ascribed to the material's capacity to regulate macrophage polarization, shifting from the pro-inflammatory M1 phenotype to the anti-inflammatory M2 phenotype, enhancing osseointegration even in inflammatory conditions.

2.4. Mechanism of CAL@PDA@GMs in promoting bone defect repair in an inflammatory environment

2.4.1. Osteogenic differentiation of BMSCs by macrophage polarization in inflammation

It is essential for bone regeneration to regulate the local immune microenvironment to facilitate the osteogenic differentiation of mesenchymal stem cells under inflammatory conditions. M1 phenotype macrophages secrete pro-inflammatory factors in the context of chronic inflammation [50], disrupting the balance between bone formation by osteoblasts and bone resorption by osteoclasts [51], which can inhibit osteogenesis following the implantation of materials. Modulating macrophage polarization towards the M2 phenotype could prevent the production of pro-inflammatory mediators, counteract anti-osteoblastic and osteolytic effects, and facilitate osteogenesis [39]. Biomaterials have been utilized to modulate various pathways associated with bone tissue formation, including the resolution of inflammation, angiogenesis, and osteogenesis, to foster the formation of new tissue, leading to bone tissue repair and improved osseointegration [37,52]. The previous findings led us to explore whether CAL@PDA@GMs could regulate osteogenic differentiation through their immunomodulatory effects. BMSCs were cultured in a conditioned medium (CM) derived from RAW 264.7 cells co-cultured with PDA@GMs or CAL@PDA@GMs (Fig. 5A). Fig. 5B–E showed that LPS^{CM}, the conditioned medium derived from LPS-stimulated cells, suppressed the ALP activity and calcium mineral

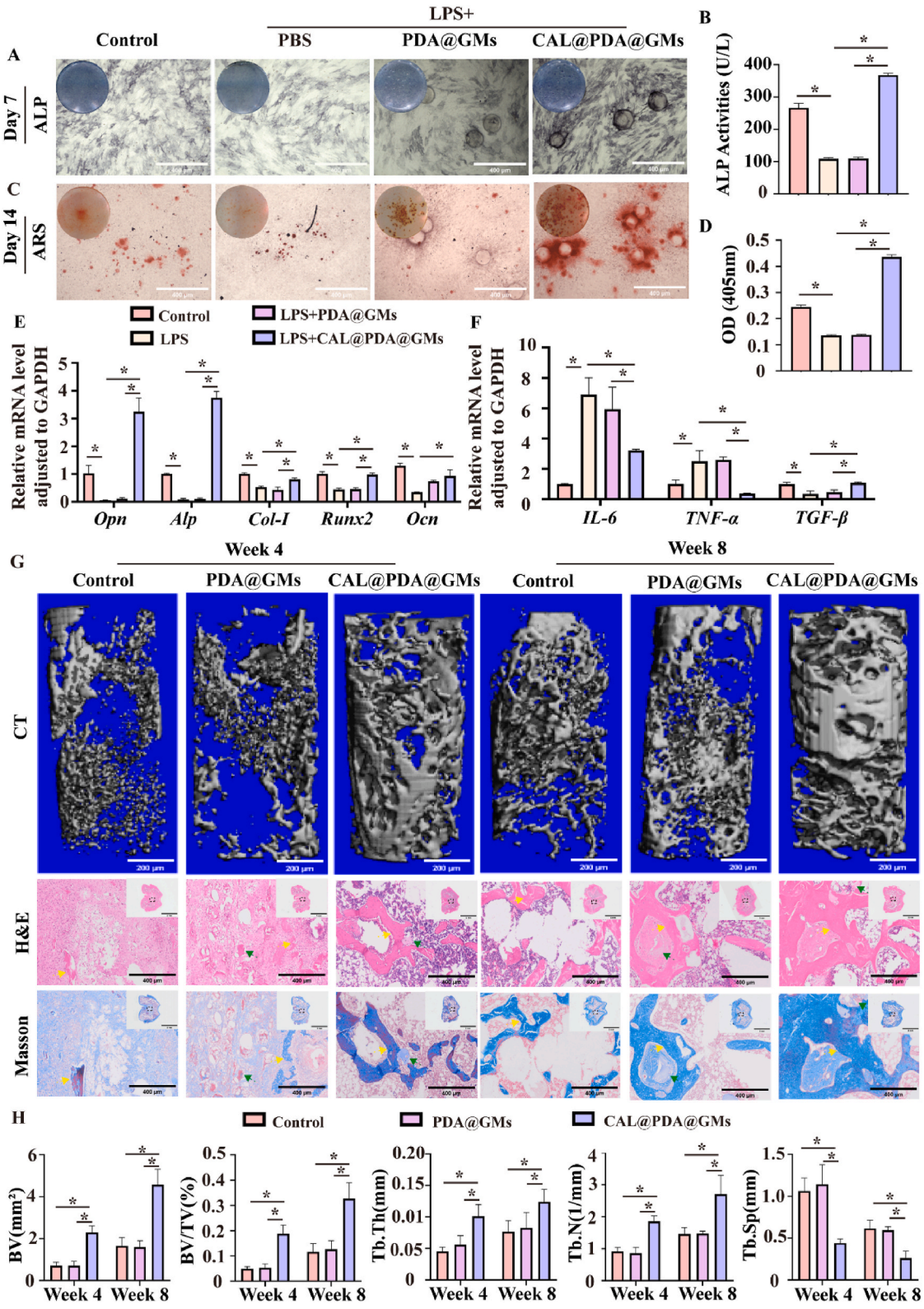

Fig. 4. Osteogenic differentiation of BMSCs in inflammation *in vitro* and bone regeneration in the rat femoral defect model in an inflammatory environment *in vivo*. A) Microscopic images and B) quantitative analysis of ALP staining on day 7. C) Microscopic images and D) quantitative analysis of ARS staining on day 14. E) Gene expression of osteogenesis-related markers (*Opn*, *Alp*, *Col-I*, *Runx2*, and *Ocn*) and F) inflammatory-related markers (*IL-6, TNF-α, TGF-β*). G) Representative micro-CT images, H&E, and Masson staining of new bone formation in the defect area 4 and 8 weeks after implantation. H) Quantitative analysis of micro-CT parameters (BV, BV/TV, Tb. N, Tb. Th, and Tb. Sp) of regenerated bone in the defect area. Yellow arrow: newly formed bone tissue. Green arrow: hydrogel. Scale bar: 400 μm (A, C), 200 μm, 5 mm, and 400 μm (G). Data are presented as the mean ± SD. *$p < 0.05$ indicates significant differences. (For interpretation of the references to colour in this figure legend, the reader is referred to the Web version of this article.)

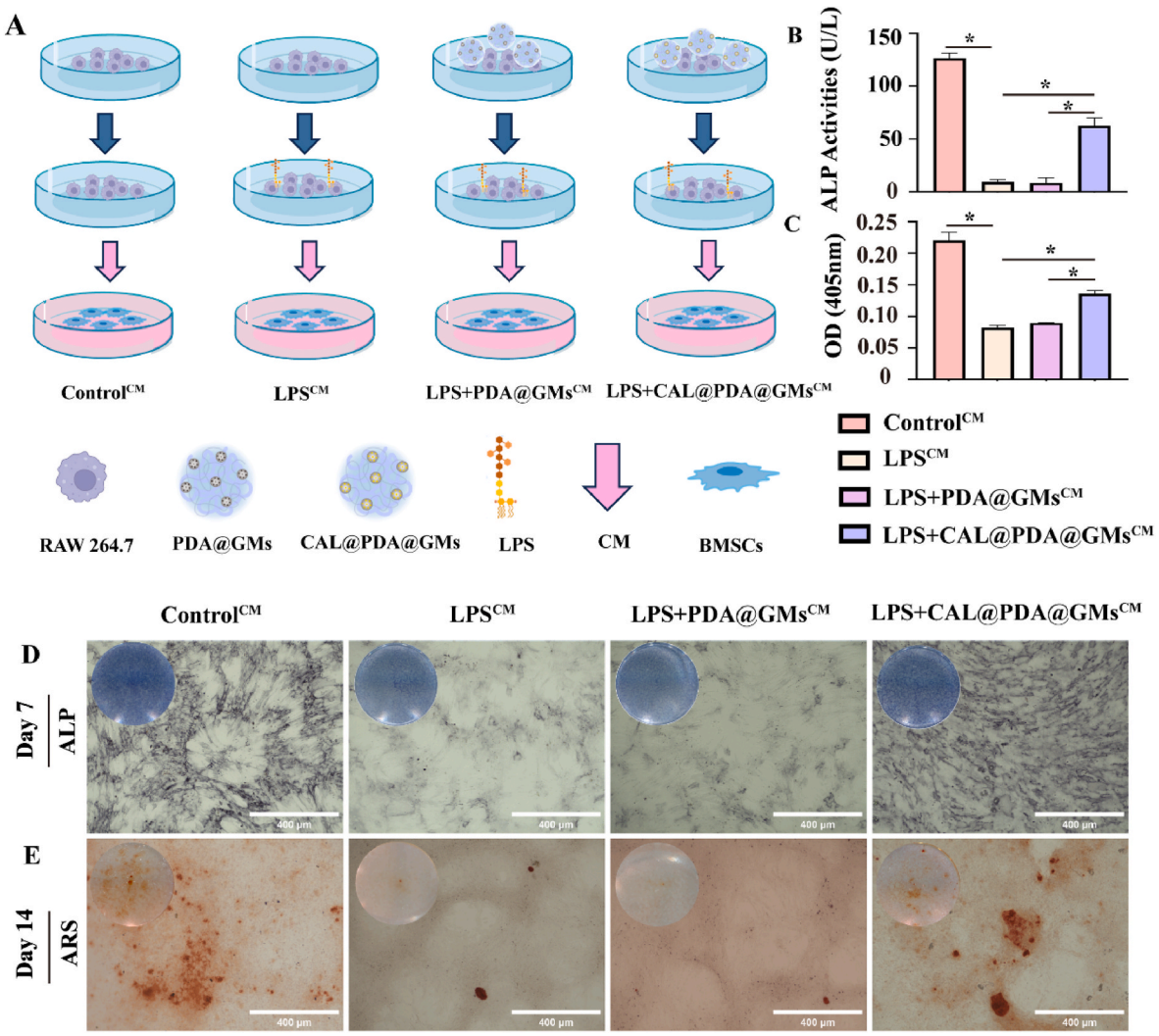

Fig. 5. Regulation of the anti-osteoblastic effects *in vitro*: A) Preparation of CM from RAW 264.7 cells. B) Quantitative analysis of ALP staining on day 7. C) Quantitative analysis of ARS staining on day 14. D) ALP and E) ARS staining microscopic images of BMSCs cultured in CM from different sources. Scale bar: 400 μm. Data are presented as the mean ± SD. $^*p < 0.05$ indicates significant differences.

deposition in BMSCs. However, this suppression was mitigated by LPS + CAL@PDA@GMs^{CM}. This suggests that CAL@PDA@GMs may promote osteogenic differentiation by creating a favorable immune microenvironment, potentially regulating macrophage polarization from the M1 to M2 phenotype.

2.4.2. *ROS scavenging performance*

Both implantation of biomaterials and surgical trauma may result in local inflammation [53]. During this process, the M1-phenotype macrophages secrete proinflammatory cytokines and ROS, which can exacerbate inflammation and increase the risk of delayed bone healing [44,53–55]. Scavenging ROS is advantageous for osteogenic differentiation. To explore the intracellular ROS scavenging capacity of CAL@PDA@GMs, we utilized the DCFH-DA probe to measure the ROS levels in RAW 264.7 macrophages stimulated by LPS. As depicted in Fig. 6A, the fluorescence intensity of DCFH-DA was elevated in the LPS group but significantly reduced in the CAL@PDA@GMs group, this was further substantiated by flow cytometry analysis (Fig. 6B and F). These results demonstrate the ROS scavenging ability of CAL@PDA@GMs, which can help protect cells from environmental oxidative stress and foster a favorable immune microenvironment conducive to bone repair. Studies have demonstrated that PDA NPs could scavenge ROS, which requires a specific concentration, and the nanoparticles should be ingested into the cell [56–58]. In this study, PDA NPs were embedded within GelMA, and the phenolic hydroxyl groups on PDA bonded with the proteins of GelMA [59,60]. This interaction not only consumed or covered some of the phenolic hydroxyl groups, reducing the opportunity to contact with ROS, but also prevented the PDA from being ingested into the cell, leading to the loss of the ROS scavenging ability of PDA@GMs [61,62]. The biofunctions of CAL@PDA@GMs can be attributed to the released calcitriol, which alleviates inflammatory processes to reduce oxidative stress damage [63,64].

2.4.3. *Macrophage polarization*

To evaluate the effect of the CAL@PDA@GMs on macrophage polarization, we used immunofluorescence staining, flow cytometry, and qRT-PCR analysis on RAW 264.7 macrophages. Fig. 6C illustrated that the LPS-treated group exhibited intense red fluorescence for CCR7, a marker of M1 macrophages, whereas the CAL@PDA@GMs group showed a stronger signal for CD206, indicative of M2 polarization. Flow cytometry results (Fig. 6D, E, G, H) echoed this trend. qRT-PCR analysis revealed a significant upregulation of pro-inflammatory/M1-related genes [*IL-1β, TNF-α*, and inducible nitric oxide synthase(*iNOS*)] in the LPS group (Fig. 6I), while anti-inflammatory/M2-related genes (*IL-10* and *TGF-β*) were significantly downregulated (Fig. 6J). Conversely, the CAL@PDA@GMs group had increased expression of anti-inflammatory/

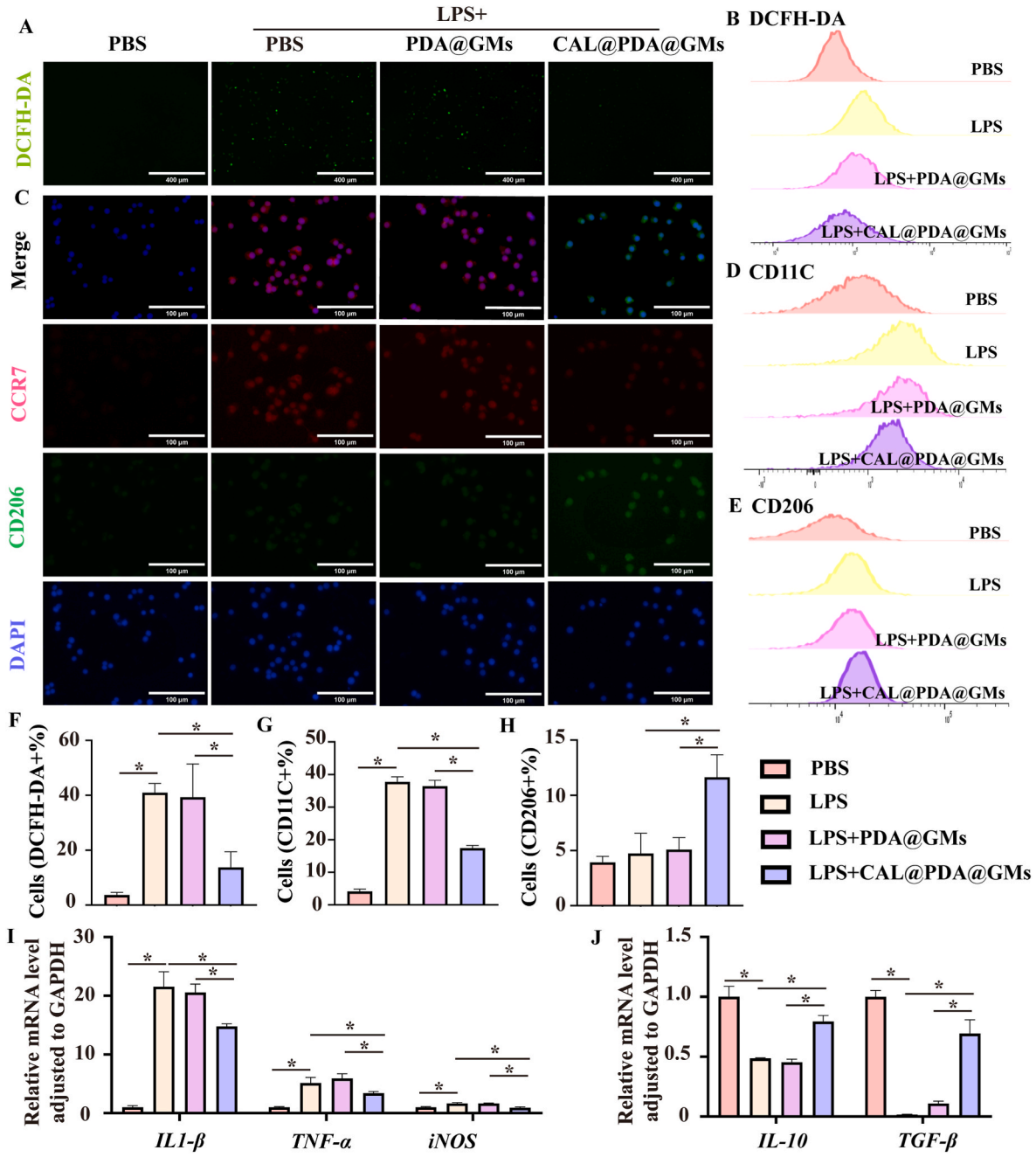

Fig. 6. Immune responses of macrophages *in vitro*. A) Representative fluorescence images and B, F) corresponding flow cytometry analysis of intracellular ROS levels. C) Representative immunofluorescence images of M1(CCR7), M2(CD206) and flow cytometry analysis of the D,G) M1(CD11C+) to E,H) M2 (CD206+) transition in RAW 264.7 cells. I) Gene expression of proinflammatory/M1 markers (*IL-1β, TNF-α, iNOS) and J) anti-inflammatory/M2 markers (IL-10, TGF-β*). Scale bar: 400 μm (A), 100 μm (C). Data are presented as the mean ± SD. $^*p < 0.05$ indicates significant differences.

M2-related genes and decreased expression of pro-inflammatory/M1-related genes.

Collectively, these findings confirm the ability of CAL@PDA@GMs to facilitate the polarization of macrophages toward the M2 phenotype, scavenge ROS, and downregulate pro-inflammatory and upregulate anti-inflammatory cytokines. CAL@PDA@GMs create a favorable immune microenvironment that supports the osteogenic differentiation of BMSCs, thereby facilitating bone defect repair under inflammatory conditions (Scheme 1B).

2.4.4. RNA-Seq verification of immunomodulation of CAL@PDA@GMs

To further reveal the potential mechanisms and associated biological processes in macrophages exposed to CAL@PDA@GMs under inflammatory conditions, we performed RNA-Seq analysis. The analysis indicated that compared to the LPS group, the CAL@PDA@GMs group exhibited a significant upregulation of 35 genes and a significant downregulation of 39 genes (Fig. 7A and C). Enrichment analysis of the Kyoto Encyclopedia of Genes and Genomes (KEGG) pathway suggested that CAL@PDA@GMs exerted a notable impact on the TNF signaling pathway, the nuclear transcription factor-kappa B (NF-κB) signaling pathway, ROS, and other inflammation-related pathways (Fig. 7D). Studies revealed that calcitriol downregulated the mitogen-activated protein kinases(MAPK) and peroxisome proliferator-activated receptor γ(PPARγ)/NF-κB/TNF-α pathway [65,66], which was the upstream pathway of NF-κB, to alleviate the inflammation [67,68]. On the other hand, ROS activates NF-κB [67], while calcitriol inhibits the

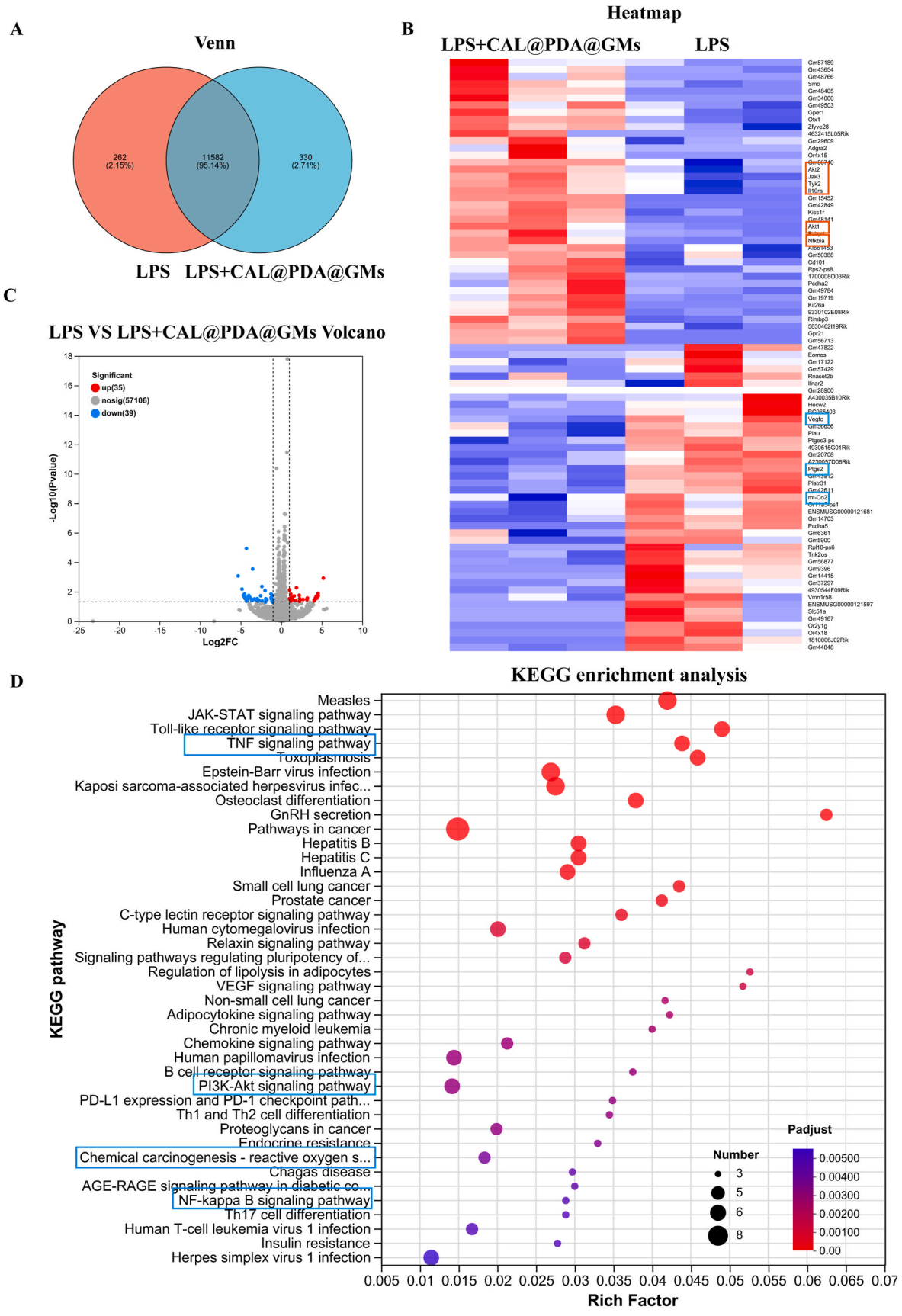

Fig. 7. Transcriptome sequencing analyses of Raw 264.7 cells stimulated by LPS treated with CAL@PDA@GMs. A) LPS with LPS + CAL@PDA@GMs Venn and B) differential genes heatmap, C) Volcano, D) KEGG enrichment analysis.

ROS-nod-like receptors 3(NLRP3)-IL-1β signaling axis against ROS [63, 64]. Among the significantly expressed differential genes, the CAL@PDA@GMs group showed a substantial downregulation of ROS-related pro-inflammatory genes (*Ptgs2, mt-Co2*) and an upregulation of anti-inflammatory genes (*IL-10ra, NFκbia*) (Fig. 7B). Combined with the qRT-PCR results, the related cytokines *IL-1β, TNF-α, iNOS, IL-10,* and *TGF-β* (Fig. 6I and J) were enriched in NF-κB and ROS signaling pathways, both of which play crucial roles in the inflammatory response. This indicates that CAL@PDA@GMs could modulate macrophage phenotypes in the inflammatory environment by targeting the NF-κB and ROS signaling pathways.

3. Conclusion

In summary, we have developed an injectable hydrogel microsphere, CAL@PDA@GMs, characterized by excellent cytocompatibility and suitable degradation properties. This microsphere sustainably releases calcitriol to promote bone regeneration, alleviate inflammation, scavenge excess ROS, and regulate macrophage polarization from M1 to M2. By optimizing immunomodulation and enhancing tissue regeneration within inflammatory environments, CAL@PDA@GMs presents a convenient, effective, and promising approach for bone regeneration, particularly in inflammatory conditions. This strategy offers significant potential as a clinical treatment for large-scale bone injuries.

CRediT authorship contribution statement

Jiajun Chen: Conceptualization, Data curation, Formal analysis, Methodology, Resources, Validation, Writing – original draft, Writing – review & editing. **Xingrui Yan:** Formal analysis, Resources, Software. **Li Nie:** Data curation, Software, Validation. **Siqi Zhou:** Investigation, Methodology, Visualization. **Ping Ji:** Conceptualization, Project administration. **Hongmei Zhang:** Funding acquisition, Project administration, Supervision.

Declaration of competing interest

The authors declare that they have no known competing financial interests or personal relationships that could have appeared to influence the work reported in this paper.

Acknowledgments

This work was funded in part by research grants from the Chongqing Traditional Chinese Medicine scientific research project (Joint project of Chongqing Health Commission and Science and Technology Bureau) (#2024ZYYB005 to HZ).

Appendix A. Supplementary data

Supplementary data to this article can be found online at https://doi.org/10.1016/j.mtbio.2025.101687.

Data availability

Data will be made available on request.

References

[1] S.J. Park, M.M. Rahman, J. Lee, et al., Investigation of bone regeneration efficacy of new bovine bone minerals in a canine mandibular critical defect model, Adv. Healthcare Mater. 12 (22) (2023) e2202942.
[2] J. Zhang, D. Tong, H. Song, et al., Osteoimmunity-regulating biomimetically hierarchical scaffold for augmented bone regeneration, Advanced Materials (Deerfield Beach, Fla.) 34 (36) (2022) e2202044.
[3] Y. Goua, K. Q, Y. W, et al., Advances of calcium phosphate nanoceramics for the osteoinductive potential and mechanistic pathways in maxillofacial bone defect repair, Nano TransMed 3 (2024) 100033.
[4] S.N. Khan, F.P. Cammisa Jr., H.S. Sandhu, et al., The biology of bone grafting, J. Am. Acad. Orthop. Surg. 13 (1) (2005) 77–86.
[5] G.L. Xu, T. Wang, C.X. Shen, et al., In-vitro physicochemical characterization of a novel type of bone defect-filling granules—BpNcCaP in comparison to deproteinized bovine bone (Bio-Oss®), Nano TransMed 2 (1) (2023) e9130016.
[6] D.S. Kim, J.K. Lee, J.H. Kim, et al., Advanced PLGA hybrid scaffold with a bioactive PDRN/BMP2 nanocomplex for angiogenesis and bone regeneration using human fetal MSCs, Sci. Adv. 7 (50) (2021) eabj1083.
[7] C. Ji, M. Qiu, H. Ruan, et al., Transcriptome analysis revealed the symbiosis niche of 3D scaffolds to accelerate bone defect healing, Adv. Sci. 9 (8) (2022) e2105194.
[8] Y. Zhu, H. Liang, X. Liu, et al., Regulation of macrophage polarization through surface topography design to facilitate implant-to-bone osteointegration, Sci. Adv. 7 (14) (2021).
[9] J. Lee, S.J. Huh, J.M. Seok, et al., Surface engineering of 3D-printed scaffolds with minerals and a pro-angiogenic factor for vascularized bone regeneration, Acta Biomater. 140 (2022) 730–744.
[10] M. Inada, K. Tsukamoto, M. Hirata, et al., Novel vitamin D3 analogs, 1alpha, 25 (OH)2D(3)-26, 23-lactam (DLAMs), antagonize bone resorption via suppressing RANKL expression in osteoblasts, Biochem. Biophys. Res. Commun. 372 (3) (2008) 434–439.
[11] Y. Ji, P. Zhang, Y. Xing, et al., Effect of 1α, 25-dihydroxyvitamin D3 on the osteogenic differentiation of human periodontal ligament stem cells and the underlying regulatory mechanism, Int. J. Mol. Med. 43 (1) (2019) 167–176.
[12] Y. Ma, J. Yang, Y. Li, et al., Effect of 1,25-dihydroxyvitamin D3 on stem cells from human apical papilla: adhesion, spreading, proliferation, and osteogenic differentiation, BioMed Res. Int. 2021 (2021) 1481215.
[13] F. Mojarad, I. Amiri, R. Rafatjou, et al., The effect of 1α,25(OH)2D3 on osteogenic differentiation of stem cells from dental pulp of exfoliated deciduous teeth, J. Dent. 17 (4) (2016) 348–353.
[14] O. Andrukhov, O. Andrukhova, U. Hulan, et al., Both 25-hydroxyvitamin-D3 and 1,25-dihydroxyvitamin-D3 reduces inflammatory response in human periodontal ligament cells, PLoS One 9 (2) (2014) e90301.
[15] D. Nebel, D. Svensson, K. Arosenius, et al., 1α,25-dihydroxyvitamin D3 promotes osteogenic activity and downregulates proinflammatory cytokine expression in human periodontal ligament cells, J. Periodontal. Res. 50 (5) (2015) 666–673.
[16] J. Zhou, F. Wang, Y. Ma, et al., Vitamin D3 contributes to enhanced osteogenic differentiation of MSCs under oxidative stress condition via activating the endogenous antioxidant system, Osteoporosis International: A Journal established as result of cooperation between the European Foundation for Osteoporosis and the National Osteoporosis Foundation of the USA 29 (8) (2018) 1917–1926.
[17] H. Liu, J. Cui, W. Feng, et al., Local administration of calcitriol positively influences bone remodeling and maturation during restoration of mandibular bone defects in rats, Materials science & engineering, C, Materials for biological applications 49 (2015) 14–24.
[18] S.J. Yoon, K.S. Park, M.S. Kim, et al., Repair of diaphyseal bone defects with calcitriol-loaded PLGA scaffolds and marrow stromal cells, Tissue Eng. 13 (5) (2007) 1125–1133.
[19] M. Zhu, Y. Shi, Y. Shan, et al., Recent developments in mesoporous polydopamine-derived nanoplatforms for cancer theranostics, J. Nanobiotechnol. 19 (1) (2021) 387.
[20] S. Mezzavilla, C. Baldizzone, K.J. Mayrhofer, et al., General method for the synthesis of hollow mesoporous carbon spheres with tunable textural properties, ACS Appl. Mater. Interfaces 7 (23) (2015) 12914–12922.
[21] M.E. Lynge, R. van der Westen, A. Postma, et al., Polydopamine–a nature-inspired polymer coating for biomedical science, Nanoscale 3 (12) (2011) 4916–4928.
[22] H. Wu, M. Wei, Y. Xu, et al., PDA-based drug delivery nanosystems: a potential approach for glioma treatment, Int. J. Nanomed. 17 (2022) 3751–3775.
[23] N. Annabi, J.W. Nichol, X. Zhong, et al., Controlling the porosity and microarchitecture of hydrogels for tissue engineering, Tissue engineering, Part B, Reviews 16 (4) (2010) 371–383.
[24] Y. Li, J. Rodrigues, H. Tomás, Injectable and biodegradable hydrogels: gelation, biodegradation and biomedical applications, Chem. Soc. Rev. 41 (6) (2012) 2193–2221.
[25] S. Xiao, T. Zhao, J. Wang, et al., Gelatin methacrylate (GelMA)-Based hydrogels for cell transplantation: an effective strategy for tissue engineering, Stem cell reviews and reports 15 (5) (2019) 664–679.
[26] X. Zhang, X. Chen, H. Hong, et al., Decellularized extracellular matrix scaffolds: recent trends and emerging strategies in tissue engineering, Bioact. Mater. 10 (2022) 15–31.
[27] A.C. Daly, L. Riley, T. Segura, et al., Hydrogel microparticles for biomedical applications, Nat. Rev. Mater. 5 (1) (2020) 20–43.
[28] J. Lin, L. Chen, J. Yang, et al., Injectable double positively charged hydrogel microspheres for targeting-penetration-phagocytosis, Small 18 (40) (2022) e2202156.
[29] J. Yang, Y. Han, J. Lin, et al., Ball-bearing-Inspired polyampholyte-modified microspheres as bio-lubricants attenuate osteoarthritis, Small 16 (44) (2020) e2004519.
[30] M. Jamshidi, C. Falamaki, Image analysis method for heterogeneity and porosity characterization of biomimetic hydrogels, F1000Research 9 (2020) 1461.
[31] Z. Xia, B. Wu, C.Y. Chan, et al., Deep-learning-based pyramid-transformer for localized porosity analysis of hot-press sintered ceramic paste, PLoS One 19 (9) (2024) e0306385.
[32] Y. Wang, Z. Yuan, Y. Pang, et al., Injectable, high specific surface area cryogel microscaffolds integrated with osteoinductive bioceramic fibers for enhanced bone regeneration, ACS Appl. Mater. Interfaces 15 (17) (2023) 20661–20676.

[33] Z. Wan, Z.Y. Yuan, Y.C. Li, et al., Hierarchical therapeutic ion-based microspheres with precise ratio-controlled delivery as microscaffolds for in situ vascularized bone regeneration, Adv. Funct. Mater. 32 (2113280) (2022) 1–16.
[34] Q. Tang, Z. Hu, H. Jin, et al., Microporous polysaccharide multilayer coated BCP composite scaffolds with immobilised calcitriol promote osteoporotic bone regeneration both in vitro and in vivo, Theranostics 9 (4) (2019) 1125–1143.
[35] L. Nie, W. Liu, J.J. Chen, et al.,A novel bioimplant comprising Ad-BMP9-transfected BMSCs and GelMA microspheres produced from microfluidic devices for bone tissue engineering, J. Tissue Eng. Regen. Med. 2023 (2023) 17.
[36] X. Li, X. Li, J. Yang, et al., Living and injectable porous hydrogel microsphere with paracrine activity for cartilage regeneration, Small 19 (17) (2023) e2207211.
[37] H. Newman, Y.V. Shih, S. Varghese, Resolution of inflammation in bone regeneration: from understandings to therapeutic applications, Biomaterials 277 (2021) 121114.
[38] C. Gao, S. Peng, P. Feng, et al., Bone biomaterials and interactions with stem cells, Bone Res. 5 (2017) 17059.
[39] J. Bai, H. Wang, H. Chen, et al., Biomimetic osteogenic peptide with mussel adhesion and osteoimmunomodulatory functions to ameliorate interfacial osseointegration under chronic inflammation, Biomaterials 255 (2020) 120197.
[40] N. Su, C. Villicana, F. Yang, Immunomodulatory strategies for bone regeneration: a review from the perspective of disease types, Biomaterials 286 (2022) 121604.
[41] Y.F. Ai, J.T. Wu, W.F. Li, et al., Hypoxia regulates BG/BMSCs@GelMA bioactive scaffolds to promote angiogenesis, osteogenesis and regulate immune responses for bone regeneration, Chem. Eng. J. 498 (2024) 154879.
[42] B. Sun, H.F. Wang, B. Xiao, et al., Bioactive composite hydrogel with effects of robust promoting osteogenesis and immunomodulation for osteoporotic bone regeneration, Chem. Eng. J. 476 (146743) (2023).
[43] J. Rui, S. Zhu, X. Xu, et al., High-performance silk/polylactic acid composite scaffold material with immunomodulation and osteogenesis function, Materials today. Bio 29 (2024) 101316.
[44] M. Wu, H. Liu, Y. Zhu, et al., Mild photothermal-stimulation based on injectable and photocurable hydrogels orchestrates immunomodulation and osteogenesis for high-performance bone regeneration, Small 19 (28) (2023) e2300111.
[45] L. Chen, J. Zhu, N. Ge, et al., A biodegradable magnesium alloy promotes subperiosteal osteogenesis via interleukin-10-dependent macrophage immunomodulation, Biomaterials 318 (2024) 122992.
[46] M. Wu, Y. Zhang, Y. Zhao, et al., Photoactivated hydrogel therapeutic system with MXene-based nanoarchitectonics potentiates endogenous bone repair through reshaping the osteo-vascularization network, Small 20 (51) (2024) e2403003.
[47] Z. Dang, W. Huang, X. Cai, et al., Dual cytokine release from microsphere-containing decellularized extracellular matrix immune regulation promotes bone repair and regeneration, Appl. Mater. Today 40 (102433) (2024).
[48] Q. Wa, Y. Luo, Y. Tang, et al., Mesoporous bioactive glass-enhanced MSC-derived exosomes promote bone regeneration and immunomodulation in vitro and in vivo, Journal of Orthopaedic Translation 49 (2024) 264–282.
[49] Z. Liu, J. Mao, W. Li, et al., Smart glucose-responsive hydrogel with ROS scavenging and homeostasis regulating properties for diabetic bone regeneration, Chem. Eng. J. 497 (154433) (2024).
[50] S.S. Rao, Y. Hu, P.L. Xie, et al., Omentin-1 prevents inflammation-induced osteoporosis by downregulating the pro-inflammatory cytokines, Bone Res. 6 (2018) 9.
[51] M. Zhu, B. Yu, J. Bai, et al., Cannabinoid receptor 2 agonist prevents local and systemic inflammatory bone destruction in rheumatoid arthritis, J. Bone Miner. Res: The official Journal of the American Society for Bone and Mineral Research 34 (4) (2019) 739–751.
[52] A. Moshaverinia, C. Chen, X. Xu, et al., Regulation of the stem cell-host immune system interplay using hydrogel coencapsulation system with an anti-inflammatory drug, Adv. Funct. Mater. 25 (15) (2015) 2296–2307.
[53] Y.Q. Huang, Z.Y. Du, k. Li, et al., ROS-scavenging electroactive polyphosphazene-based core–shell nanofibers for bone regeneration, Advanced Fiber Materials 4 (2022) 894–907.
[54] M. Lian, B. Sun, Y. Han, et al., A low-temperature-printed hierarchical porous sponge-like scaffold that promotes cell-material interaction and modulates paracrine activity of MSCs for vascularized bone regeneration, Biomaterials 274 (2021) 120841.
[55] M. Wu, H. Liu, D. Li, et al., Smart-responsive multifunctional therapeutic system for improved regenerative microenvironment and accelerated bone regeneration via mild photothermal therapy, Adv. Sci. 11 (2) (2024) e2304641.
[56] X. Bao, J. Zhao, J. Sun, et al., Polydopamine nanoparticles as efficient scavengers for reactive oxygen species in periodontal disease, ACS Nano 12 (9) (2018) 8882–8892.
[57] Z. Wu, K. Yuan, Q. Zhang, et al., Antioxidant PDA-PEG nanoparticles alleviate early osteoarthritis by inhibiting osteoclastogenesis and angiogenesis in subchondral bone, J. Nanobiotechnol. 20 (1) (2022) 479.
[58] L. Bai, Y. Wang, K. Wang, et al., Materiobiomodulated ROS therapy for de novo hair growth, Advanced materials (Deerfield Beach, Fla.) 36 (21) (2024) e2311459.
[59] J. Saiz-Poseu, J. Mancebo-Aracil, F. Nador, et al., The chemistry behind catechol-based adhesion, Angew. Chem. 58 (3) (2019) 696–714.
[60] H. Zhang, T.Y. Zhao, B. Newland, et al., Catechol functionalized hyperbranched polymers as biomedical materials, Prog. Polym. Sci. 78 (2018) 47–55.
[61] N. Yang, T. Wu, M. Li, et al., Silver-quercetin-loaded honeycomb-like Ti-based interface combats infection-triggered excessive inflammation via specific bactericidal and macrophage reprogramming, Bioact. Mater. 43 (2025) 48–66.
[62] Y.L. Yu, J.J. Wu, C.C. Lin, et al., Elimination of methicillin-resistant Staphylococcus aureus biofilms on titanium implants via photothermally-triggered nitric oxide and immunotherapy for enhanced osseointegration, Military Medical Research 10 (1) (2023) 21.
[63] C. Cui, C. Wang, F. Jin, et al., Calcitriol confers neuroprotective effects in traumatic brain injury by activating Nrf2 signaling through an autophagy-mediated mechanism, Molecular medicine (Cambridge, Mass.) 27 (1) (2021) 118.
[64] Y. Dai, J. Zhang, J. Xiang, et al., Calcitriol inhibits ROS-NLRP3-IL-1β signaling axis via activation of Nrf2-antioxidant signaling in hyperosmotic stress stimulated human corneal epithelial cells, Redox Biol. 21 (2019) 101093.
[65] X. Li, S. Xu, J. Liu, et al., Treatment with 1,25-dihydroxyvitamin D3 delays choroid plexus infiltration and BCSFB injury in MRL/lpr mice coinciding with activation of the PPARγ/NF-κB/TNF-α pathway and suppression of TGF-β/Smad signaling, Inflammation 46 (2) (2023) 556–572.
[66] X. Li, J. Liu, Y. Zhao, et al., 1,25-dihydroxyvitamin D3 ameliorates lupus nephritis through inhibiting the NF-κB and MAPK signalling pathways in MRL/lpr mice, BMC Nephrol. 23 (1) (2022) 243.
[67] B. Hu, H. Zhang, X. Meng, et al., Aloe-emodin from rhubarb (Rheum rhabarbarum) inhibits lipopolysaccharide-induced inflammatory responses in RAW264.7 macrophages, J. Ethnopharmacol. 153 (3) (2014) 846–853.
[68] K. Qian, L. Shan, S. Shang, et al., Manganese enhances macrophage defense against Mycobacterium tuberculosis via the STING-TNF signaling pathway, Int. Immunopharmacol. 113 (Pt B) (2022) 109471.